Theor Chem Acc (1999) 101:319–324
DOI 10.1007/s00214980m174

Theoretical
Chemistry Accounts

Regular article

Interaction energy anisotropy of the pyrrole dimer: ab initio theoretical study

Vladimír Lukeš[1], **Martin Breza**[2], **Stanislav Biskupič**[2]

[1] Department of Chemical Physics, Slovak Technical University, SK-81237 Bratislava, Slovakia
[2] Department of Physical Chemistry, Slovak Technical University, SK-81237 Bratislava, Slovakia

Received: 11 June 1998 / Accepted: 6 October 1998 / Published online: 1 February 1999

Abstract. The van der Waals pyrrole dimer is studied using supermolecular and perturbation ab initio treatment with inclusion of correlation energy. The influence of selected geometry variations on the interaction energy components is investigated. Our calculations verified the minimum on the potential energy surface deduced from microwave spectra. Its stability is possibly related not to the extremal values of the selected interaction energy contributions but its physical origin is connected with the delicate equilibrium between the repulsive and attractive forces. Any structure variation connected with the extremal attraction energy is more than compensated for by the repulsion energy.

Key words: Pyrrole dimer – Weak molecular interactions – Perturbation theory

1 Introduction

The investigation of simple aromatic ring π systems is very attractive from the experimental as well as from the theoretical point of view. Knowledge of these weak van der Waals (vdW) interactions helps us to understand better more complicated processes resulting in the packing of aromatic molecules in crystals, the tertiary structure of proteins, the base-base interaction within two DNA chains or the reaction mechanism between biologically active compounds and biomolecules [1, 2].

The vdW complexes formed from two benzene or pyrrole monomers serve as a typical example of the above-mentioned interactions. Based on experimental data, the optimum structure of the benzene dimer interplane angle is proposed to be 70°–90° [3, 4]. Further studies on isotopomers revealed the existence of more than one conformer [5]. Consequently, theoretical investigations have tried to localise all the important minima on the potential energy surface (PES) [6–10] and so verify the suggested conformations. Less symmetric systems such as benzene-CO [11] and benzene-N_2 [12] have also been investigated.

Columberg and Bauder [13] recently reported the first detailed experimental study of the rotational spectrum of the pyrrole dimer. Different isotopomers were investigated in a pulsed molecular jet. Apart from the nuclear hyperfine interaction, no further splitting or perturbations of the rotational energy levels were observed. The transition frequencies followed the pattern of an asymmetric rotor with centrifugal distortion. These facts were interpreted as a clear indication that the dimer is associated with a single local minimum on the PES. The transition frequencies were accurately fitted to a set of rotational and centrifugal distortion constants for each isotopomer. The planar moments of inertia of all isotopomers were used to derive the critical parameters of the dimer structure. The orientation of the pyrrole monomers was found to be analogous to the T-shaped structure of the benzene dimer. The centres of mass for the monomers were separated by 7.778(6) a.u. [0.4116(3) nm]. The ring planes of the monomers were at an angle of 55.42(42)° to each other (Fig. 1). The smaller angle for the two pyrrole molecules indicates that the equilibrium structure tends more to a displaced antiparallel rather than to a rigorous T-shaped orientation of the monomers as was expected from considerations of simple dipole-dipole interactions.

The N-H hydrogen of the monomer (oriented towards the π-electron system of the other monomer) is located 4.308 a.u. (0.228 nm) above the ring plane, indicating substantial hydrogen bonding [13]. The good agreement between the spectroscopically determined dissociation energy (estimated in a pseudodiatomic approximation) [13] of 0.0027 hartree (7.1 kJ/mol) and the enthalpy of dimerization of pyrrole in CCl_4 solution of −0.0022 to −0.0029 hartree (−5.9 to −7.5 kJ/mol) determined from nuclear magnetic resonance measurements [14] is most likely fortuitous (the zero-point energy correction is neglected) [13].

The anisotropy of the total interaction energy depends on a delicate balance between the attractive and

Correspondence to: V. Lukeš
e-mail: lukes@theochem.chtf.stuba.sk

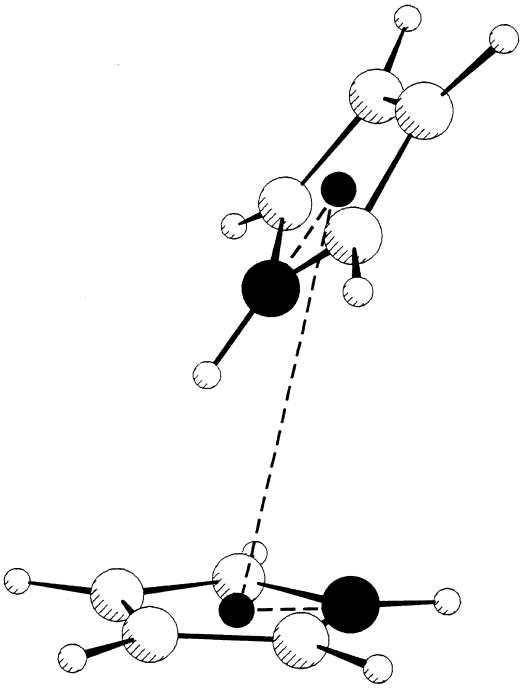

Fig. 1. Experimental structure of the pyrrole dimer. *Open circles* denote carbon (*large*) and hydrogen (*small*) atoms, the *full circles* denote nitrogen atoms (*large*) and centre-of-mass positions (*small*) of individual pyrrole rings

repulsive interaction energy contributions. The decomposition of the interaction energy enables us to analyse which fundamental components determine the anisotropy in a particular region. The aim of this paper is to verify the suggested experimental structure of the vdW pyrrole dimer using a theoretical ab initio treatment. Additional investigation of the influence of geometry variations near the experimental vdW minimum on the changes of the individual energy contributions might be helpful for a better understanding of the physical principles of weak bonding not only in biological systems.

2 Theory

The interaction energy can be calculated using the supermolecular or perturbation treatment [15, 16]. In the supermolecular method, it is evaluated as the sum of the self-consistent field (SCF) interaction energy (ΔE^{SCF}) and the correlation interaction energy. In this work the correlation components will be determined at the second-order Møller–Plesset theory (MP2) level. The intermolecular perturbation theory (IPT) calculates the interaction energy directly as the sum of the electrostatic, exchange-penetration, induction, dispersion, etc. energies:

$$E^{\mathrm{int}} = E_{\mathrm{elst}} + E_{\mathrm{exch\text{-}pn}} + E_{\mathrm{ind}} + E_{\mathrm{disp}} + \cdots . \tag{1}$$

Each of these components has a different physical origin, properties and behaviour with respect to the intermolecular degree of freedom. The common problem in IPT is the antisymmetry of the supersystem wave function with respect to all electrons. The methods for the inclusion of the exchange effects are, in principle, of two types [17].

1. The symmetry adapted perturbation theories (SAPT), where the zero-order wave function is represented by the simple product of the zero-order wave functions of the isolated systems and the proper symmetry is ensured in each order of the perturbation expansion [18–20].

2. The symmetric perturbation theories, where the zero-order wave function has the correct symmetry with respect to all electrons [21–24].

The additional separation of the supermolecular interaction energy can be provided using the perturbation calculation of the interaction energy components. Thus the SCF interaction energy is decomposed into a component usually referred to as the Heitler–London (HL) energy ΔE^{HL} (sum of the electrostatic and first-order exchange-penetration energies) [25] and the deformation SCF energy $\Delta E^{\mathrm{SCF}}_{\mathrm{def}}$ [26, 27]. The induction and exchange-induction energies are present in the last term. In some IPT versions an additional type of "charge-transfer" energy contribution is also included in the Hartree–Fock (HF) deformation part [16].

The basic decomposition of the interaction correlation MP2 energy leads to the separation of the second-order HF dispersion energy ($E^{(20)}_{\mathrm{disp}}$), second-order exchange-dispersion energy ($E^{(20)}_{\mathrm{ex\text{-}disp}}$) and the remaining contributions [16, 18].

$$\Delta E^{(\mathrm{MP2})} = E^{(20)}_{\mathrm{disp}} + E^{(20)}_{\mathrm{ex\text{-}disp}} + E^{(2)}_{\mathrm{other}} \tag{2}$$

The last term ($E^{(2)}_{\mathrm{other}}$) contains the electrostatic correlation correction, as well as the intra- and intermonomer correlation components contributing to the deformation effects [16].

3 Basis set and geometry specifications

The selection of the basis set for the description of vdW complexes is a very complicated task. This has to take into account different aspects such as the dipole and quadrupole moments, polarisability, charge distributions, basis set superposition error (BSSE) and the economy of calculations. We have used the smaller basis sets (Table 1) for the separation of basic interaction energy contributions, whereas the double-zeta polarised (DZP) basis set (Table 1) was only applied for the verification of general trends.

The supermolecular interaction energy was calculated using the MOLCAS 3 package [28]. The atomic one- and two-electron integrals, SCF orbital energies and molecular orbitals generated by the GAUSSIAN 92 package [29] were applied to the evaluation of the SAPT energy contributions [20] as well as for the HL and induction-polarisation energies calculated using the orthogonalised orbitals [24]. The BSSE was eliminated via the standard counterpoise procedure of Boys and Bernardi [30]. The perturbation interaction energy contributions were obtained employing the basis set of the whole dimer (the dimer-centred basis set) [16].

The pyrrole dimer systems were studied in the experimental geometry (Fig. 1) as well as in geometries described in Table 2. The centre-of-mass distance $d(\mathrm{X_C\text{-}Y_C})$ between the proton-acceptor (X) and the proton-donor (Y) molecule was varied for the experimental geometry symmetry, whereas in the remaining systems (A–E) it was fixed to the value of 7.778 a.u. [13]. Some preliminary calculations related to supermolecule energy minimisation in DZP basis sets have also been performed for parallel-displaced and T-shaped structures. The structure of the individual pyrrole molecules was taken from Ref. [31].

Table 1. Calculated values of the Hartree–Fock energy, dipole moment and polarisability for the pyrrole monomer with the basis sets under study. We chose the coordinate system with the pyrrole molecule in the *xy*-plane, the positive *x*-axis along N-H bond and the origin at the centre of mass. All values are in atomic units

No.	Basis set	Ref.	E^{SCF}	μ	α_{xx}	α_{yy}	α
1	C-MINI N-MINI H-MINI	[32]	−207.133 335	1.9931	−21.69	−23.98	29.15
2	C-MIDI N-MIDI H-MINI	[32]	−207.449 659	1.9931	−21.69	−23.98	37.05
3	C-3-21G N-3-21G H-3-21G	[33]	−207.646 256	1.9975	−17.40	−19.41	35.82
4	C-DZP N-DZP H-DZP	[33]	−208.850 036	2.0028	−17.33	−19.79	42.57
	Experimental	[34, 35]		1.74			55.8

Table 2. The equilibrium centre-of-mass distances and the stabilisation energy data for the geometry of experimental orientation with the basis set of Table 1

Basis set	Centre-of-mass distance (a.u.)	Dissociation energy (μhartree)
1	8.05	−7407.2
2	8.20	−4975.3
3	8.23	−7165.4
4	8.05	−8560.0
Experimental [13]	7.778	−2697.4

4 Results and discussion

The basis set influence on E^{SCF}, dipole moment and polarisability (both calculated at the HF level) of the isolated pyrrole molecule is illustrated in Table 1 and is compared with experimental data [34, 35]. In contrast to the dipole moment, the polarisability is much more sensitive to the quality of the basis sets. As expected, the smaller basis sets underestimate the values of the polarisability. The larger basis set (4) produces better results.

The experimental structure symmetry was confirmed as the most stable one. The equilibrium centre-of-mass distances and the stabilisation energy data are listed for the geometry of experimental orientation with the basis sets used in Table 2. The distance obtained comes near to the experimental value with increasing size of the basis set used. The dissociation energy, however, does not exhibit this trend. (Table 2).

In analogy with Ref. [9] we started the supermolecule geometry optimisation at the MP2 level with parallel-displaced structures. Mutual pyrroles rotation leads to the most stable antiparallel orientation. Further energy decrease is associated with their mutual shift to a lower N_X-N_Y distance [$d(X_C$-$Y_C) = 6.80$ a.u., angles N_X-X_C-$Y_C = X_C$-Y_C-$N_Y = 56.4°$, see Fig. 2a]. However, this energy minimum is related only to a special cut of the PES for parallel structures and corresponds to the saddle point on the complete PES. The complete optimisation leads to the structure near the experimental configuration.

Similar investigations have been done with T-shaped structures. The Y pyrrole rotation around its symmetry axis gives the most stable configuration perpendicular to mirror plane of the X one. Further energy lowering is connected with the Y pyrrole shift along the symmetry axis of the Y molecule to higher N_X-N_Y distances [$d(X_C$-$Y_C) = 8.14$ a.u., angles N_X-X_C-$Y_C = 95.4°$ and X_C-Y_C-$N_Y = 5.4°$, see Fig. 2b]. This energy is 470 μhartree lower (at the MP2 level) than for the optimum parallel-displaced structure. Analogously, as in the previous case, the complete optimisation leads to the structure near the experimental configuration (Y pyrrole wagging).

In contrast to the benzene dimer [9], there is only a single global minimum on the pyrroles PES. This might be explained by lower pyrrole molecular symmetry (C_{2v}) in comparison with benzene (D_{6h}). Nevertheless, the mirror plane is preserved in optimum configurations of both dimers.

Our results indicate that the total interaction energy is less dependent on the rotation around the axis perpendicular to the pyrrole plane (cf. B and C geometries of Table 3 and Fig. 3). If the rotation axis is not perpendicular to the pyrrole plane, proton shifting into the neighbouring molecule occurs, which is associated with the repulsion energy increase (cf. E2 and A geometries of Table 3 and Fig. 3). The minimum interaction energy corresponds to the experimental geometry except for basis set 2 with the most stable C geometry. This is caused by too large a difference between the experimental and the optimum geometry corresponding to this basis set.

In the following discussion the various contributions to the interaction energy for the structures studied are considered. Let us recall that ΔE^{SCF} contains the ΔE^{HL} and the HF deformation terms. Evidently ΔE^{HL} (open symbols in Fig. 3) may acquire both positive (with superiority of the exchange-penetration contributions) and negative (with superiority of the electrostatic contribution) values. This is clearly demonstrated in Fig. 4 where the electrostatic ($E^{(10)}_{elst}$, full symbols) and first-order SAPT exchange-penetration components ($E^{(10)}_{exch}$, open symbols) are distinguished. As in Ref. [16] the electrostatic energy at the SCF level for polar systems is shown to be a very unstable term. The exchange contribution is relatively stable and comes closer to the limiting value with basis size extension than the coulombic one.

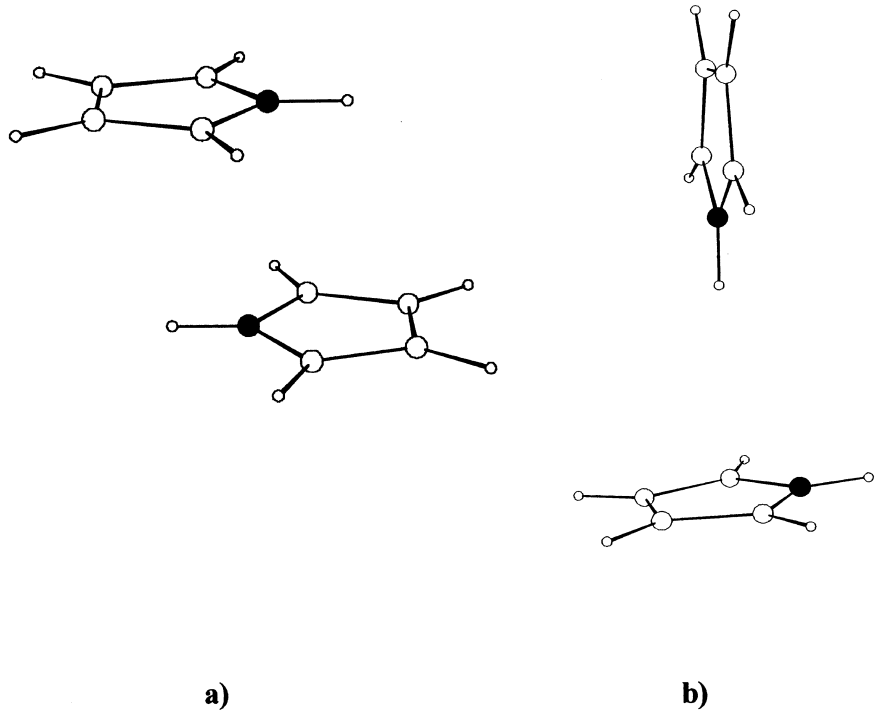

Fig. 2a,b. Calculated structures of **a** optimum parallel-displaced and **b** T-shaped structures of the pyrrole dimer

Table 3. Geometries of the pyrrole dimer systems under study (X_C and Y_C are the centre-of-mass positions; X and Y refer to the proton-acceptor and proton-donor pyrrole molecules, respectively, see Fig. 1)

Geometry	Dihedral angles (deg)			Bond angles (deg)	
	$(C_\alpha\text{-}N)_X\text{-}X_C\text{-}Y_C$	$N_X\text{-}X_C\text{-}Y_C\text{-}N_Y$	$X_C\text{-}Y_C\text{-}(N\text{-}C_\alpha)_Y$	$N_X\text{-}X_C\text{-}Y_C$	$X_C\text{-}Y_C\text{-}N_Y$
Exp.	90	180	90	78	22.6
A	78	180	90	78	22.6
B	90	168	90	78	22.6
C	90	180	78	78	22.6
D_1	90	180	90	90	22.6
D_2	90	180	90	66	22.6
E_1	90	180	90	78	34.6
E_2	90	180	90	78	10.6

The magnitude of the induction-polarisation part of the interaction energy may be estimated as $\Delta E_{\text{def}}^{\text{SCF}}$ or as the sum of the HF coulombic ($E_{\text{ind}}^{(20)}$) and relevant exchange-induction ($E_{\text{ex-ind}}^{(20)}$) terms [20]. The important attractive component $E_{\text{ind}}^{(20)}$ can be decomposed into the induction interaction $E_{\text{ind}}^{(20)}(\text{Y} \rightarrow \text{X})$ of the X monomer with the static field of the Y monomer and $E_{\text{ind}}^{(20)}(\text{X} \rightarrow \text{Y})$ defined vice versa. The coupling of the electron exchange with the induction interaction of the X(Y) monomer with the static field of the Y(X) monomer is approximated by the $E_{\text{ex-ind}}^{(20)}$ term. Analogously, $E_{\text{ex-ind}}^{(20)}(\text{Y} \rightarrow \text{X})$ and $E_{\text{ex-ind}}^{(20)}(\text{X} \rightarrow \text{Y})$ contributions may be distinguished here. The total monomer induction energies for the induction-polarisation of the proton-acceptor [$E_{\text{ind}}^{(20)}(\text{Y} \rightarrow \text{X}) + E_{\text{ex-ind}}^{(20)}(\text{Y} \rightarrow \text{X})$, see Fig. 5] and proton-donor [$E_{\text{ind}}^{(20)}(\text{X} \rightarrow \text{Y}) + E_{\text{ex-ind}}^{(20)}(\text{X} \rightarrow \text{Y})$, see Fig. 6] pyrrole molecules are denoted by full symbols. The D1 geometry (quasi-T shape) is connected with the best charge induction from proton-donor to proton-acceptor pyrrole (Fig. 5). These trends are supported by the monomer

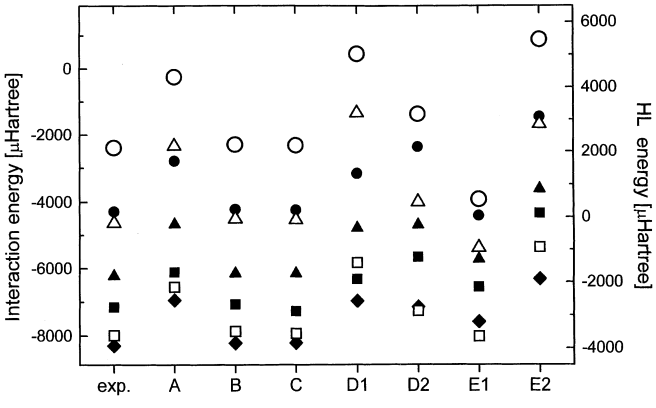

Fig. 3. Interaction (*full symbols*, *left axis*) and Heitler–London (*HL*) energies (*open symbols*, *right axis*) for the geometries under study (Table 3) calculated with basis sets 1 (*squares*), 2 (*circles*) and 3 (*triangles*) of Table 1

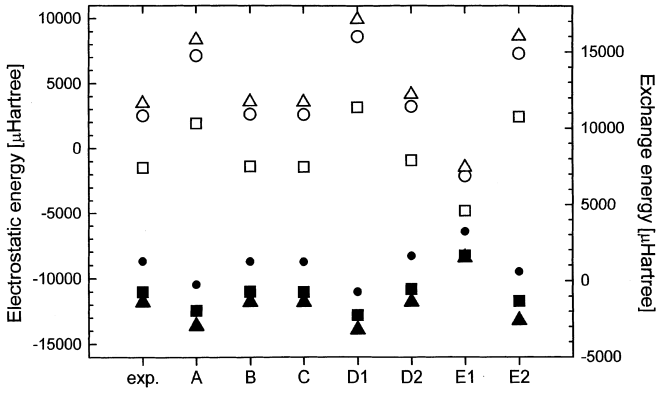

Fig. 4. Electrostatic ($E^{(10)}_{\mathrm{elst}}$) (*full symbols*, *left axis*) and exchange ($E^{(10)}_{\mathrm{exch}}$) energy values (*open symbols*, *right axis*) for the geometries under study (Table 3) calculated with basis sets 1 (*squares*), 2 (*circles*) and 3 (*triangles*) of Table 1

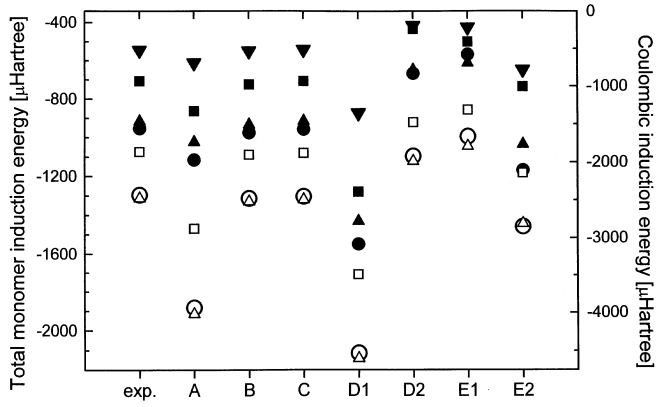

Fig. 5. Total monomer induction $[E^{(20)}_{\mathrm{ind}}(\mathrm{Y}\rightarrow\mathrm{X})+E^{(20)}_{\mathrm{ex\text{-}ind}}(\mathrm{Y}\rightarrow\mathrm{X})]$ (*full symbols*, *left axis*) and monomer coulombic-induction $[E^{(20)}_{\mathrm{ind}}(\mathrm{Y}\rightarrow\mathrm{X})]$ energy values (*open symbols*, *right axis*) for the geometries under study (Table 3) calculated with basis sets 1 (*squares*), 2 (*circles*) and 3 (*triangles*) of Table 1. *Inverted triangles* denote the monomer induction energies based on the perturbation theory treatment using the orthogonalised basis sets

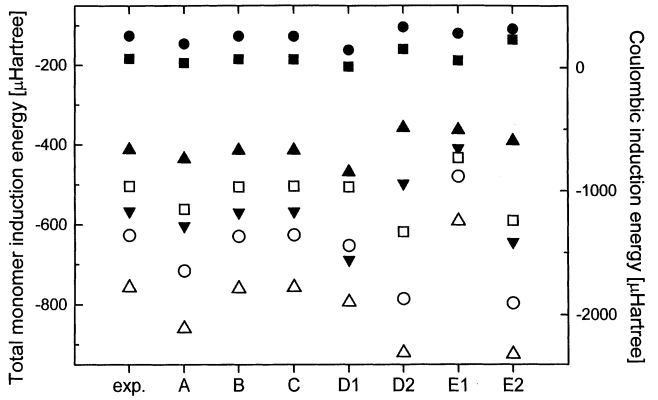

Fig. 6. Total monomer induction $[E^{(20)}_{\mathrm{ind}}(\mathrm{X}\rightarrow\mathrm{Y})+E^{(20)}_{\mathrm{ex\text{-}ind}}(\mathrm{X}\rightarrow\mathrm{Y})]$ (*full symbols*, *left axis*) and monomer coulombic-induction $[E^{(20)}_{\mathrm{ind}}(\mathrm{X}\rightarrow\mathrm{Y})]$ energy values (*open symbols*, *right axis*) for the geometries under study (Table 3) calculated with basis sets 1 (*squares*), 2 (*circles*) and 3 (*triangles*) of Table 1. *Inverted triangles* denote the monomer induction energies based on the perturbation theory treatment using the orthogonalised basis sets

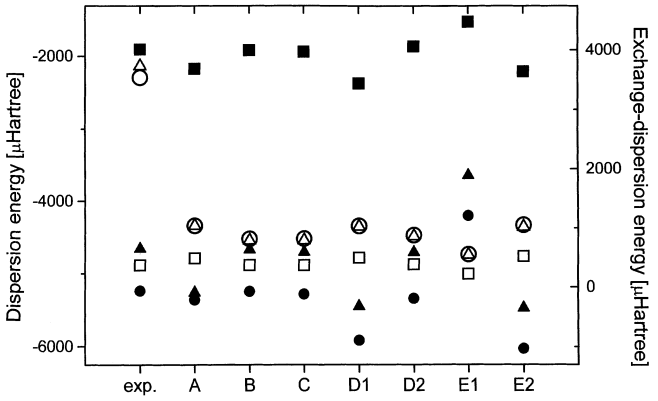

Fig. 7. Dispersion ($E^{(20)}_{\mathrm{disp}}$) (*full symbols*, *left axis*) and exchange-dispersion ($E^{(20)}_{\mathrm{ex\text{-}disp}}$) energy values (*open symbols*, *right axis*) for the geometries under study (Table 3) calculated with basis sets 1 (*squares*), 2 (*circles*) and 3 (*triangles*) of Table 1

induction energies based on the perturbation theory treatment using the orthogonalised basis sets for basis set 3 (full inverted triangles in Figs. 5, 6). The delicate equilibrium between HF coulombic (open symbols in Figs. 5, 6) and exchange contributions which are included in the total induction energy (full symbols in Figs. 5, 6) is evident especially for the A, D1/D2 and E2 geometries.

Similarly, ΔE^{MP2} plays an important role in the anisotropy of the total interaction energy. The dispersion energy ($E^{(20)}_{\mathrm{disp}}$) contained in this term is the dominant attractive component, whereas the exchange-dispersion energy ($E^{(20)}_{\mathrm{ex\text{-}disp}}$) is the leading repulsive one. The dispersion energy (denoted by full symbols in Fig. 7) significantly depends on the basis set type. The small basis set (1) overestimates the HF electrostatic energy (denoted by full symbols in Fig. 4) but it provides small values of the HF dispersion energy. The behaviour of $E^{(20)}_{\mathrm{ex\text{-}disp}}$ is illustrated in Fig. 7 (open symbols) and its trend is opposite to the $E^{(20)}_{\mathrm{disp}}$ one. This has a smoothing effect on the anisotropy of their sum.

Here the question arises why the pyrrole dimer in the experimental geometry exhibits the highest stability. Our results indicate that this stability is related not to the extremal values of the selected interaction energy contributions but that its physical origin is connected with the delicate equilibrium between the repulsive and attractive forces. The corresponding energies are usually in the medium-value range (cf. Figs. 3–7). Any structure variation connected with the extremal attraction energy is more than compensated for by the repulsion energy (i.e. the coulombic and exchange energy of D1 in Fig. 4).

5 Conclusions

Our introductory quantum-chemical calculations on the pyrrole dimer in the geometries varied near the exper-

imental minimum were not performed at the "chemical accuracy" level (0.001 hartree $\approx$ 0.6 kcal/mol) due to technical problems (disk space limitations). It is necessary to note that the difference between the spectroscopic dissociation energy [13] and the one calculated in our paper is within the estimated uncertainties originating naturally from the limitations in the basis sets and electron correlation treatment employed. It is well known [9] that only higher level calculations covering triple excitations performed with extended basis sets posses reasonably accurate stabilisation energies. However, this significantly increases the requirements on computer capacity for large systems. Nevertheless, preliminary calculations with basis set 3 of Table 1 indicate that the contributions of the third- and fourth-orders (singlet, doublet and quadruplet) of perturbation theory are repulsive and cause a shift of the total interaction energy (see Table 3) by about 14% towards the experimental value. In order to perform such calculations at higher theoretical levels, the appropriate basis set to be used has to be tested at least at the MP2 level. According to our results one of the important criteria for its quality is that it must not overestimate the electrostatic contributions to the detriment of the exchange ones (cf. Figs. 3–7).

We have examined the ability of several dominant interaction energy contributions to reproduce the experimental structure and the binding energy of the pyrrole dimer. The significance of the attractive intermolecular forces and their leading role is clearly demonstrated (see the contributions to the HF induction and dispersion energies). On the other hand, the HL energy (sum of the HF electrostatic and relevant exchange-penetration energies) can have either attractive or repulsive character, depending on the dimer geometry.

It can be concluded that the interaction of two polar subsystems such as pyrrole rings leads to a system where the dipole moments play an important part but not the dominant one: as in the benzene dimer [8, 9], the significant role belongs to the dispersion forces.

Further studies on the importance of higher interaction-correlation energy contributions as well as on the predictive investigation of the other, probably less stable pyrrole dimer conformers and the saddle points of the PES are desirable.

Acknowledgements. The work reported in this paper has been funded by the Slovak Grant Agency, project nos. 1/4205/97 and 1/4199/97.

References

1. Hobza P, Zahradník R (1988) Intermolecular complexes. Academic Press, Prague
2. Hobza P, Zahradník R (1988) Chem Rev 88:871
3. Bömsen KO, Selzle HL, Schlag EW (1986) J Chem Phys 85:1726
4. Henson BF, Hartland GV, Venturo VA, Felker PM (1992) J Chem Phys 97:2189
5. Scherzer W, Krätzschmar O, Selzle HL, Schlag EW (1992) Z Naturforsch A47:1248
6. Hobza P, Selzle HL, Schlag EW (1990) J Chem Phys 93:5893
7. Hobza P, Selzle HL, Schlag EW (1993) J Phys Chem 97:3937
8. Hobza P, Selzle HL, Schlag EW (1994) J Am Chem Soc 116:3500
9. Hobza P, Selzle HL, Schlag EW (1994) Chem Rev 94:1767
10. Smith GD, Jaffe RL (1996) J Phys Chem 100:9624
11. Brupbacher T, Bauder A (1993) J Chem Phys 99:9394
12. Ohshima Y, Kohguchi H, Endo Y (1991) Chem Phys Lett 184:21
13. Columberg G, Bauder A (1997) J Chem Phys 106:504
14. Perkampus H, Krüger U, Krüger W (1969) Z Naturforsch B 24:1365
15. Kolos W (1983) In: Löwdin PO, Pulman B (eds) New horizons of quantum chemistry. Reidel, Dortrecht, pp 243–277
16. Chalasiński G, Szcześniak MM (1994) Chem Rev 94:1723
17. Jeziorski B, Kolos W (1982) In: Ratajczak H, Orvile-Thomas WJ (eds) Molecular interactions, vol 3. Wiley, New York, pp 1–46
18. Rybak S, Jeziorski B, Szalewicz K (1991) J Chem Phys 95:6576
19. Moszyński R, Jeziorski B, Szalewicz K (1994) J Chem Phys 100:1312
20. Jeziorski B, Moszyński R, Ratkiewicz A, Rybak S, Szalewicz K, Wiliams HL (1993) In: Clementi E (ed) Methods and techniques in computational chemistry, vol B. METECC-94 STEF, Cagliari, pp 79–126
21. Kvasnička V, Laurinc V, Hubač I (1974) Mol Phys 42:1345
22. Daudey JP, Claverie P, Malerieu JP (1974) Int J Quantum Chem 8:1
23. Surján PR, del valle CP (1996) Theor Chim Acta 94:333
24. Laurinc V. Lukeš V, Biskupič S (1998) Theor Chem Acc 99:53
25. Jeziorski B, Bulski M, Piela L (1976) Int J Quantum Chem 10:281
26. Moszynski R, Heijmen TGA, Jeziorski B (1996) Mol Phys 88:741
27. Lukeš V, Laurinc V, Biskupič S (1999) Int J Quantum Chem (in press)
28. Anderson K, Blomberg MRA, Fülscher MP, Karlström G, Kellö V, Lindh R, Malmqvist P-A, Noga J, Olsen J, Roos BO, Sadlej AJ, Siegbahn PEM, Urban M, Widmark P-O (1994) MOLCAS-3. University of Lund, Sweden
29. Frisch MJ, Trucks GW, Head-Gordon M, Gill PMW, Wong MW, Foresman JB, Johnson BG, Schlegel HB, Robb MA, Replogle ES, Gomperts R, Andres JL, Raghavachari K, Binkley JS, Gonzales C, Martin RL, Fox DJ, Defrees DJ, Baker J, Stewart JJP, Pople JA (1992) GAUSSIAN 92. Gaussian, Pittsburgh, Pa
30. Boys SF, Bernardi F (1970) Mol Phys 19:553
31. Nygaard L, Tielsen JT, Kirchheiner J, Maltesen G, Rastrup-Andersen J, Sørensen GO (1969) J Mol Struct 3:491
32. Huzinaga S (1984) In: Andzelm J, Klobukowski E, Radzio-Andzelm E, Sakai Y, Tatewaki H (eds) Gaussian basis sets for molecular calculations. Elsevier, Amsterdam, pp 4–86
33. Dupuis M, Watts JD, Villar HO, Hunt GJB (1988) Program HONDO/7. QCPE 544
34. Christen D. Griffiths JH, Scheriden J (1982) Z Naturforsch A 37:1378
35. Le Févre CG, Le Févre RJW, Rao BP, Smith MR (1959) J Chem Soc 1188